ACS SENSORS

pubs.acs.org/acssensors

Article

Hybrid Integrated Cardiomyocyte Biosensors for Bitter Detection and Cardiotoxicity Assessment

Xinwei Wei, Deming Jiang, Changming Chen, Jianguo Wu, Chunlian Qin, Qunchen Yuan, Yingying Xue, Yizhou Xiong, Liujing Zhuang,* Ning Hu,* and Ping Wang*

Cite This: *ACS Sens.* 2021, 6, 2593−2604

Read Online

ACCESS | Metrics & More | Article Recommendations | Supporting Information

ABSTRACT: Among basic taste sensations, bitter taste is vital to the survival of mammals due to its indispensable role in toxin prediction or identification, so the identification of bitter compounds is of great value in the pharmaceutical and food industry. Recently, bitter taste receptor (T2Rs)-based biosensors have been developed for specific bitter detection. However, the taste biosensors based on taste cells/tissues suffer from simple function, low sensitivity, low content, and limited parameters. Here, to establish a high-content, highly sensitive, and multifunctional taste biosensor, we developed a multifunctional hybrid integrated cardiomyocyte biosensor (HICB) for bitter detection. Due to the expression of bitter taste receptors in cardiomyocytes, the HICB can recognize the specific bitter agonists by synchronously recording the extracellular field potential (EFP) and mechanical beating (MB) signals from the cultured cardiomyocytes in vitro. Multiple feature parameters were defined and extracted from the electromechanical signals of cardiomyocytes to analyze the specific responses to four typical bitter compounds. The radar map, heat map, and principal component analysis (PCA) were used to visualize and classify the specific responses. Moreover, bitter-induced cardiotoxicity also was chronically evaluated, and these bitter compounds presented an inhibition effect on the electrophysiological and contractile activities of cardiomyocytes. This high-content HICB offers an alternative platform for both bitter detection and cardiotoxicity assessment, showing promising applications in the fields of taste detection and toxicity screening.

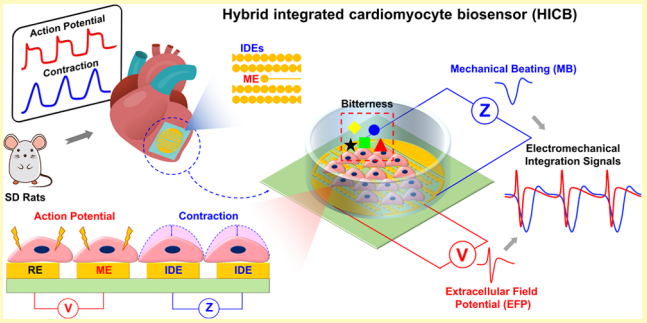

KEYWORDS: *hybrid integrated cardiomyocyte biosensor, cardiomyocyte, taste biosensor, bitter detection, cardiotoxicity assessment*

Taste, also called gustation, plays a significant role in nutrient and toxin detection for feeding or breeding in five basic sensations in mammals.[1] Currently, sour, sweet, bitter, salty, and umami have been widely regarded as basic taste sensations.[2,3] Among these basic taste sensations, the bitter taste can be applied for toxin identification, which is vital to the survival of mammals, thus making it indispensable in taste perception.[4,5] Therefore, the electronic tongues for bitter detection, which mimic the biological taste sensing system of mammals, have received great attention for their high-potential applications in the fields of food safety, environmental monitoring, and pharmaceutical investigation.[6−9] These electronic tongues, which usually employ electrochemical, optical, mass, and enzymatic as the sensitive elements to build the biosensors, show some merits in specific bitter detection. However, the sensitivity and specificity of these artificial electronic tongues are still far from the native biological taste system of mammals. Therefore, bionic biosensors employing gustatory bioactive components have attracted wide attention for bitter detection in recent years.[10,11]

In the taste system of mammals, bitter perception begins with the interactions between bitter compounds and type II cells in taste buds, which is mediated by a subfamily of G-protein-coupled receptors (GPCRs) known as bitter receptors T2Rs/T2rs (taste receptor, type II).[12] The activation of T2Rs induced by specific bitter ligands could lead to a series of intracellular and extracellular responses of electrophysiology and biochemistry.[13] Consequently, due to the unique physiological activity and specificity, cells or tissues that express T2Rs were applied as sensitive elements of taste sensors for bitter detection. For example, mouse germ cells and Caco-2 cells (human intestinal cell line), expressing T2Rs endogenously, as well as HEK-293 cell lines transfected with T2Rs have been used as sensitive elements for bitter investigation and detection.[14−19]

In our previous study, rat cardiomyocytes were combined with the microelectrode array (MEA) to establish a taste

Received: January 24, 2021
Accepted: June 28, 2021
Published: July 12, 2021

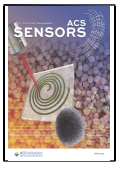

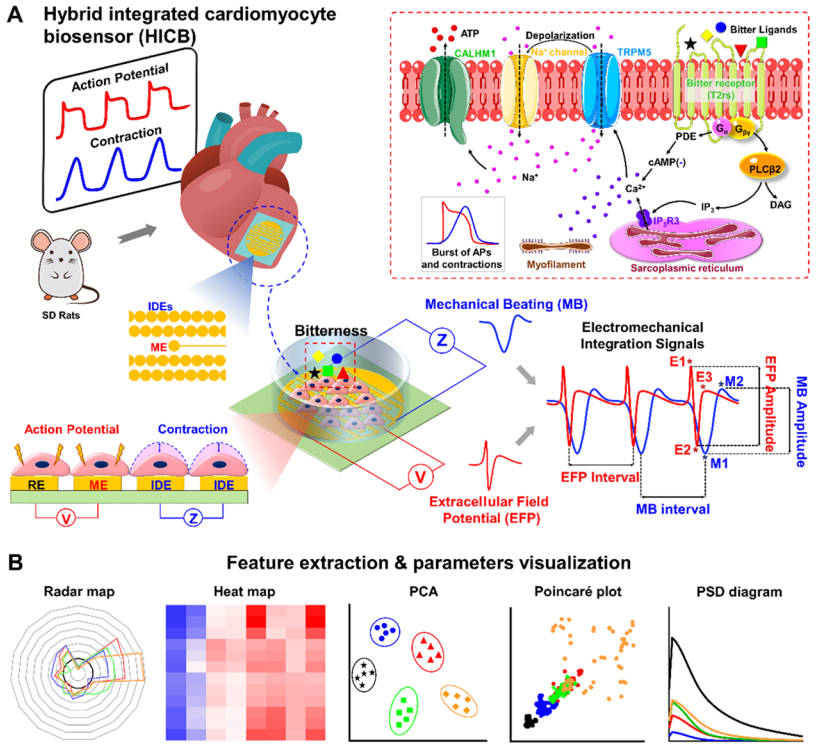

Figure 1. Schematics of the high-content hybrid integrated cardiomyocyte biosensor (HICB). (A) Establishment and detection principle of HICB. (B) Multiple feature extraction and parameter visualization for high-content analysis.

biosensor for the first time,[20] which has advantages of quick bitter detection. However, this method can only provide single electrical signals of cardiomyocytes for bitter compound recognition, while other important characteristics of cardiomyocytes, mechanical contractile signals, were ignored. Recent studies have demonstrated that the bitter taste receptor agonists possessed a negative effect on cardiac contractility.[21,22] Therefore, it is very interesting and promising to simultaneously investigate the bitterness by electrophysiological signals and mechanical contractile signals of cardiomyocytes. Moreover, about 60% of the bitter compounds in nature have documented toxicity,[23] while the studies on bitter-induced cardiotoxicity are still limited. So, it is necessary and important to assess the potential cardiotoxicity of bitter compounds, which may help to understand the mechanism of bitterness. With the rapid development of micro/nanomanufacturing and biosensing technology, cardiomyocyte-based biosensors have emerged as an effective tool to study the physiological function of the heart in vitro and have been widely used in the fields of drug discovery, toxicology, and cardiovascular diseases.[24,25]

In this study, we proposed a novel hybrid integrated cardiomyocyte biosensor (HICB) for bitter detection and cardiotoxicity assessment, where the extracellular field potential (EFP) and mechanical beating (MB) signal of cardiomyocytes can be synchronously recorded by the hybrid integrated biosensor (Figure 1). Four types of bitter agonists (denatonium benzoate/Dena, diphenidol, quinine, and arbutin) that can activate different bitter receptors in cardiomyocytes were administrated to the HICB, and HICB can quickly respond to bitter stimulation. To perform a high-content bitter evaluation, multiple feature parameters were defined based on the characteristics of recorded electromechanical signals. Subsequently, these extracted parameters were visualized by radar map, heat map, and principal components analysis (PCA) for specific bitter recognition. Further, the cardiotoxicity of bitter compounds was also chronically evaluated by HICB. It is believed that our HICB will provide a powerful platform for taste investigation and pharmaceutical applications.

METHODS AND EXPERIMENTS

Sensor Fabrication. Sensor fabrication processes refer to standard microfabrication processes (Figure S1A). The sensor device was fabricated on a 4-inch quartz glass wafer (Pyrex Corning 7740 glass). The microelectrodes (MEs) and interdigitated electrodes (IDEs) were integrated on the same sensor chip, where the reference electrodes were placed on two sides (Figure S1B). The Ti/Au (10/100 nm) electrode pattern was defined by photolithography, sputtering, and lift-off processes. Subsequently, the SiO_2/Si_3N_4 passivation pattern was fabricated by the PECVD process and wet etching. A customized polystyrene chamber was assembled on the integrated device for cell culture, and the device was then fixed on a printed circuit board (PCB) to connect with a homemade detection system (Figure S1C).

Detection of Electromechanical Signals. The detection principle of electromechanical signals of cardiomyocytes is shown in Figure 1A. Microelectrodes and IDEs of HICB were in charge of recording EFP and MB signals, respectively. First, using electrical cell−substrate impedance sensing (ECIS) technology, growth and MB signals of cardiomyocytes can be monitored by IDEs. To be specific, an alternating current (AC) voltage with an amplitude of 10 mV and a frequency of 10 kHz was applied to the IDEs, and a stable ion current was generated between two pairs of IDEs. This ion current can be influenced by the impedance changes of IDEs due to cell attachment, cell proliferation, and cell morphology, termed as the cell index (CI) value ($CI = \Delta Z/Z_0$), which reflects the ratio of the impedance changes (ΔZ) to baseline impedance (Z_0). Furthermore, rhythmic mechanical contraction of cardiomyocytes could also cause cell morphology changes, making it possible to acquire the MB signals from the impedance changes of IDEs. By increasing the speed sampling to 500 Hz, the high temporal resolution of impedance

https://doi.org/10.1021/acssensors.1c00158
ACS Sens. 2021, 6, 2593−2604

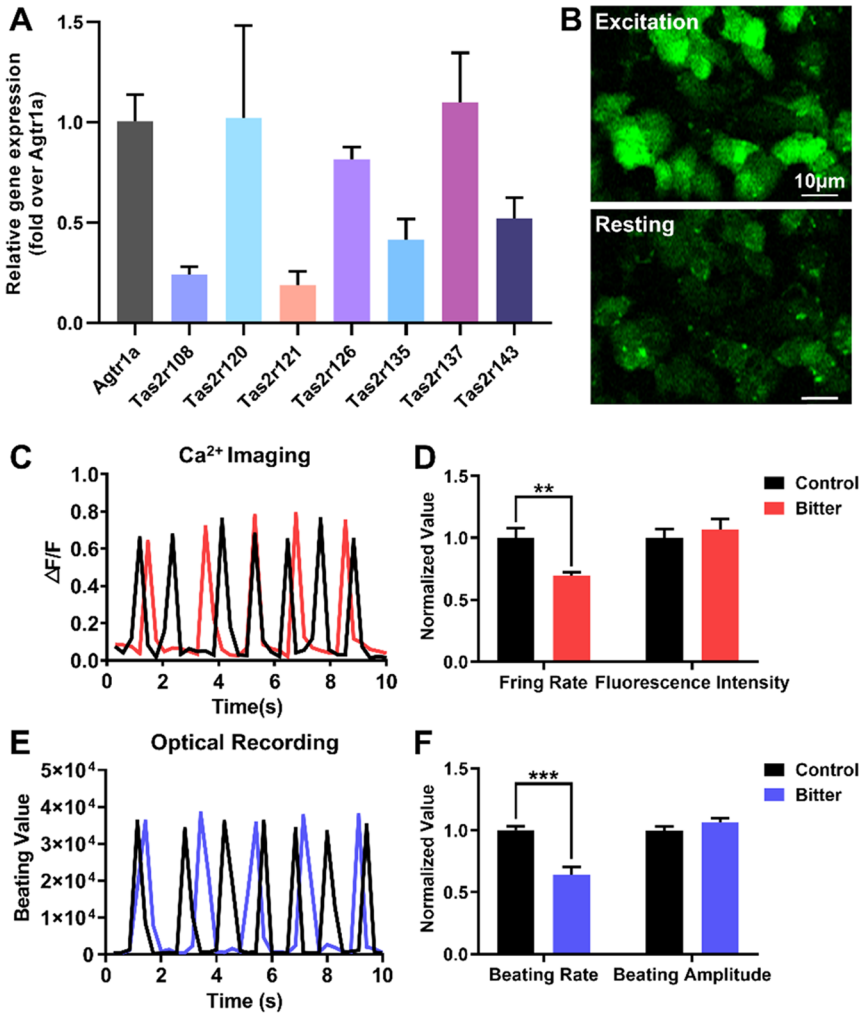

Figure 2. Bitter receptor expression in cardiomyocytes and the response of cardiomyocytes to bitter compounds. (A) Expression levels of bitter receptors (T2r108, T2r120, T2r121, T2r126, T2r135, T2r137, and T2r143) on cardiomyocytes determined by RT-qPCR, $n = 3$; (B) Ca^{2+} imaging of cardiomyocytes in the resting and exciting status; (C) Ca^{2+} fluorescence intensity curves of cardiomyocytes before and after bitter treatment; (D) statistics of the firing rate and fluorescence intensity of Ca^{2+} imaging, $n = 3$; (E) optical recording signals of cardiomyocytes beating before and after treatment with bitter compounds; and (F) statistics of the beating rate and beating amplitude of optical recording, $n = 3$ (**$P < 0.01$; ***$P < 0.001$).

signals for viewing the mechanical beating of cardiomyocytes can be achieved. At the same time, action potentials of cardiomyocytes induced by Na^+, K^+, and Ca^{2+} current can be recorded as EFP signals by microelectrodes distributed between the IDEs, and the following signal processing circuits can filter out the applied voltages and eliminate the influence of electrical interference. Therefore, this novel hybrid integrated biosensor can achieve the synchronized electro-mechanical integration recording of cardiomyocytes.

Cell Culture. The cell culture protocol is the same as the previous study.[26,27] Briefly, the ventricular tissues were isolated from 1−2 day old Sprague−Dawley rats (SD rats), and tissues were then cut into 1 mm^3 fragment. The cell suspension was prepared after enzymatic dissociation and centrifugation, and purified cardiomyocytes were obtained after twice differential attachment treatment. After seeding cells on the sensor chip, the whole integrated device was fixed on the detection system that was placed in a cell incubator, and the medium was changed every day. All protocols complied with the regulations of Zhejiang University and Sun Yat-sen University Institutional Animal Care and Use Committee (IACUC).

RT-qPCR. Total RNA was extracted from isolated cardiomyocytes by TRIZOL reagent (Macherey-Nagel, Germany). Extracted RNA was reverse-transcribed to cDNA using a 5X RT Buffer (Toyobo, Japan) and then subjected to PCR amplification using the Fast qPCR Mix kit (Takara, Japan) (95 °C for 30 s, followed by 40 cycles of 95 °C for 5 s and 60 °C for 30 s) with a CFX connect system (Bio-Rad). The primers and probes were chemically synthesized by Sangon Biotech (China) and are listed in Table S1.

Live−Dead Staining. Calcein-AM (Invitrogen) and propidium iodide (PI, Invitrogen) were used to check the live and dead status of cardiomyocytes on the integrated device, respectively. After 20 min staining, phosphate-buffered saline (PBS) (Solarbio, China) was used to rinse the samples. Subsequently, fluorescent images were taken by an inverted fluorescent microscope (NIB900, Nexcope) in a dark environment.

Immunofluorescence Staining. Immunofluorescence staining was performed on the cell nuclei and α-actin of cardiomyocytes. The isolated cardiomyocytes were washed with PBS (0.01 M) and then fixed with 4% paraformaldehyde (PFA, Solarbio, China) at room temperature for 30 min. Rinsed by PBS three times, the cells were permeabilized with 0.15% Triton X-100 (Aladdin) for 15 min and then incubated with a blocking solution of 1% bovine serum albumin (BSA, Gibco) for 30 min at 37 °C. Then, the cells were incubated with the primary antibody (monoclonal anti-α-actin) in a 4 °C refrigerator overnight. After three times rinsing with PBS, cells were then incubated with secondary antibodies (Cy3-labeled goat anti-mouse IgG (H + L)) at room temperature for 2 h. Finally, DAPI

https://doi.org/10.1021/acssensors.1c00158
ACS Sens. 2021, 6, 2593−2604

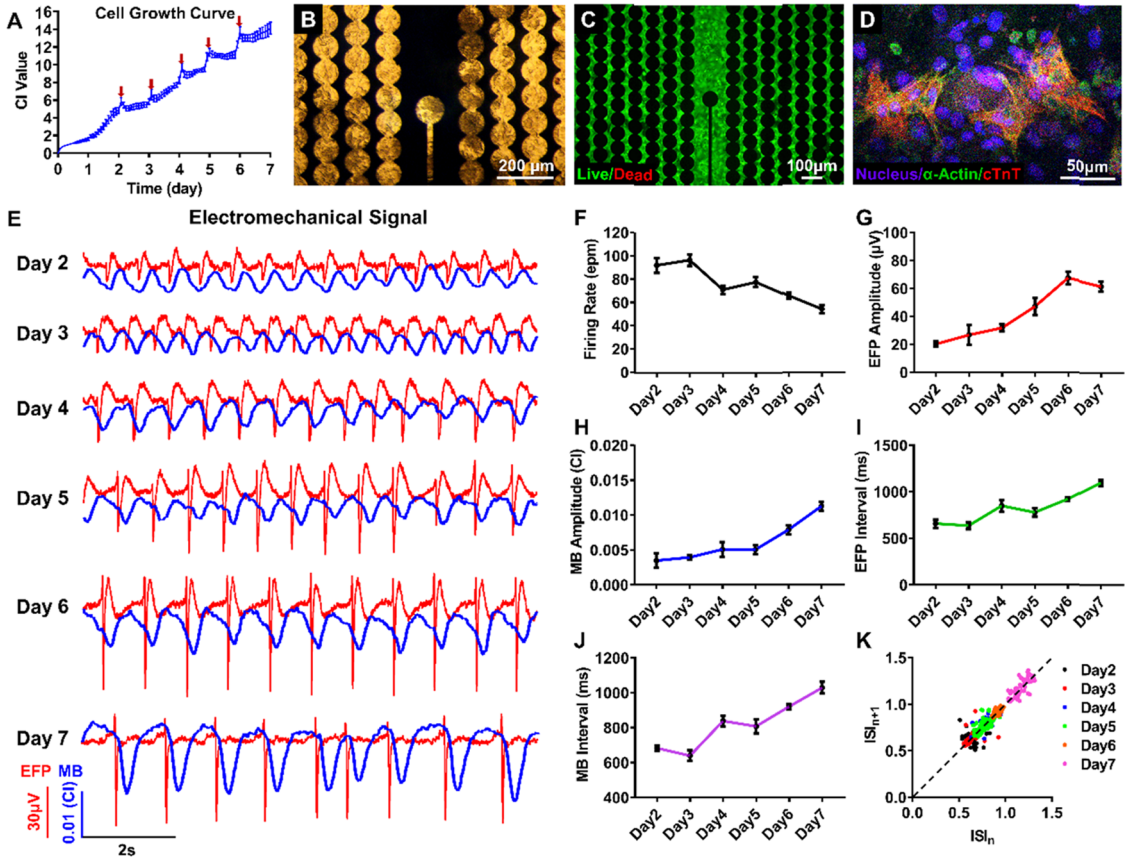

Figure 3. Establishment and optimization of the hybrid integrated cardiomyocyte biosensor (HICB). (A) Cell growth curves of cardiomyocytes on HICB (red arrow, replacing culture medium every 24 h); (B) optical microscopy images of cardiomyocytes on HICB under an upright microscope; (C) live/dead staining results of cardiomyocytes on HICB under an inverted fluorescence microscope; (D) immunofluorescence staining results of primary cardiomyocytes (purple, nucleus; green, α-actin; red, cTnT); (E) typical extracellular field potential (EFP) and mechanical beating (MB) signals of cardiomyocytes from day 2 to day 7; (F–J) statistics of the firing rate, EFP amplitude, MB amplitude, EFP interval, MB interval time; and (K) Poincaré plots of data recorded in different days.

(Solarbio, China) was used to stain the nuclei of cardiomyocytes for 10 min, and the fluorescence images of cell nuclei and α-actin were obtained by laser confocal fluorescence microscopy (NIKON, Japan).

Calcium Imaging. The culture medium was removed, and the cardiomyocytes were washed with Hanks' balanced salt solution (HBSS, Gibco). Subsequently, 5 μM Fluo-4 AM (Gibco; maximum absorption, 494 nm; maximum emission, 506 nm) working solution was added to cover the cells and incubated at 37 °C for 30 min. Following that, the working solution was removed, and cells were rinsed and maintained in HBSS for 20 min. Dena (100 μM) was used as the testing bitter compound and added to cardiomyocytes. Calcium signals were observed under a fluorescence microscope (NIKON, Japan), and the recorded videos were further analyzed by MATLAB (MathWorks).

Optical Recording. To compare with the method of mechanical beating detection by the ECIS method, the optical recording method using video microscopy was used. First, the mechanical beating video of cardiomyocytes was recorded in real time by microscopy. Then, the target cells were marked in the video for detection. Finally performing the edge detection algorithm to track the changes of the cell edge. The cell edge will change when cardiomyocytes generate periodic contraction and relaxation. Therefore, the mechanical beating of cardiomyocytes can be reflected by detecting the cell edge.

Feature Extraction and Data Analysis. To quantify the signal characteristics, feature parameters including the firing rate (FR), EFP amplitude, MB amplitude, EFP interval, and MB interval were extracted for analysis. Moreover, based on the features of the electromechanical signals of cardiomyocytes, E1, E2, and E3 were defined to label the peak, valley, and second peak points of electrical signals, respectively, while M1 and M2 were defined as the peak and valley points of mechanical signals, respectively (Figure 1A). The time interval between different feature points can be calculated to characterize the signals. Signal processing and filtering and principal components analysis (PCA) were all performed by customized MATLAB programs. The results were presented as mean ± SD (standard deviation). Data were performed using GraphPad Prism 8 (GraphPad Software Inc.), SPSS 10.0 (SPSS Inc.), and Excel 2016 (Microsoft Corporation).

RESULTS

Characterization of Bitter Taste Receptor Expression in Cardiomyocytes. To confirm the expression of bitter taste receptors in rat cardiomyocytes, the expression levels of these seven bitter taste receptors (T2r108, T2r120, T2r121, T2r126, T2r135, T2r137, and T2r143) were verified by RT-qPCR in this study. As shown in Figure 2A, the expression levels of all seven bitter taste receptors are comparable to another GPCR, the angiotensin II type 1a receptor (Agtr1a). Among these bitter receptors, the expression quantities of T2r120, T2r126, and T2r137 are relatively higher than those of other receptors. As shown in the calcium imaging results (Figure 2B), the Ca^{2+} fluorescence intensity of cardiomyocytes changed with Ca^{2+} transient due to the excitation–contraction coupling (ECC) of cardiomyocytes. When cardiomyocytes generate electrical excitation, the intracellular Ca^{2+} concentration will increase sharply due to the calcium-induced calcium release mecha-

https://doi.org/10.1021/acssensors.1c00158
ACS Sens. 2021, 6, 2593–2604

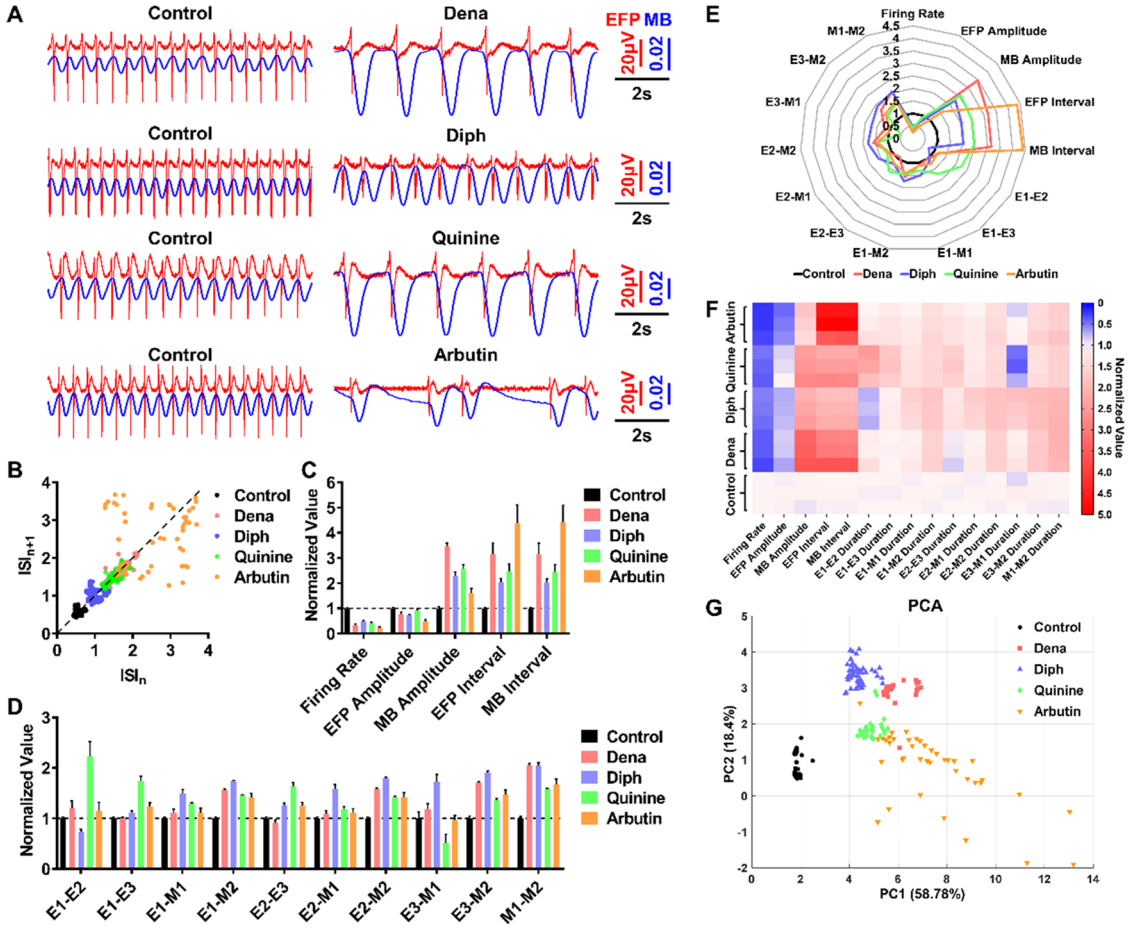

Figure 4. Quick responses of the hybrid integrated cardiomyocyte biosensor (HICB) to different bitter compounds. (A) Typical electromechanical signals of cardiomyocytes treated with different bitter compounds; (B) Poincaré plots of data after treatment with different bitter compounds; (C) normalized statistics of extracted parameters, $n = 3$; (D) normalized statistics of duration time between different feature points, $n = 3$; (E) radar map for extracted parameter visualization; (F) heat map for extracted parameter visualization; and (G) two-dimensional (2D) pattern clustering results based on principal component analysis (PCA).

nism, resulting in a stronger intensity of Ca^{2+} fluorescence compared with the resting state. To verify activation of the bitter receptors in cardiomyocytes, a common bitter compound Dena (which can activate T2r135) was chosen as the test compound, and the Ca^{2+} activities of cardiomyocytes were characterized by calcium imaging. Figure 2C shows the dynamic Ca^{2+} fluorescence intensity curves before and after adding bitter compounds to cardiomyocytes. From the results, it can be found that the firing rate of cardiomyocytes decreased after the bitter addition, demonstrating that bitter compounds can reduce the electrical excitation activities of cardiomyocytes by affecting calcium activity. Based on the statistics of the firing rate and fluorescence intensity (Figure 2D), it is indicated that the administration of bitter compounds presented a significant inhibition effect on the firing rate of cardiomyocytes, which was consistent with former studies.[21,22] Moreover, the results of optical recording of cardiomyocyte beating also showed a similar manner (Figure 2E). The beating rate of cardiomyocytes decreased after treatment with bitter compounds, while the beating amplitude presented a slight increase (Figure 2F).

Establishment and Optimization of the Hybrid Integrated Cardiomyocyte Biosensor. Cardiomyocytes from neonatal SD rats were employed to establish HICB. Cell culture medium was replaced every day. The cell growth and electromechanical activity of cardiomyocytes were synchronously monitored by HICB. Figure 3A shows the cell growth curve of cardiomyocytes during consecutive 7 days. The increase of CI indicated the cell attachment and growth, while the fluctuation of the curve is caused by medium replacement. From the optical microscopy images of cardiomyocytes on day 7 (Figure 3B), it was observed that cells were attached and uniformly distributed on the surface of the sensor device. Meantime, live/dead staining results verified the good viability of cells (Figure 3C), which demonstrates the good biocompatibility of the device and the safety of measuring technologies. In addition, the immunofluorescence staining results verified the characteristics of primary cardiomyocytes, where the nucleus was labeled in purple, α-actin was labeled in green, and cTnT was labeled in red (Figure 3D).

Figure 3E shows the typical recorded electromechanical signals within 7 days. It can be found that the amplitudes of EFP and MB signals increased and gradually reached a stable physiological status with time. To evaluate the status of cardiomyocytes quantitatively and comprehensively, basic parameters including the firing rate, EFP amplitude, MB amplitude, EFP interval, and MB interval were derived and analyzed from the recorded signals. As shown in Figure 3F, it can be found that the firing rate decreased from 92.5 ± 6.41 events/min on day 2 to 54.3 ± 3.51 events/min on day 7,

https://doi.org/10.1021/acssensors.1c00158
ACS Sens. 2021, 6, 2593−2604

while the EFP amplitude (Figure 3G) and MB amplitude (Figure 3H) increased from 20.22 ± 1.95 μV and 0.0035 ± 0.001 (CI) to 61.9 ± 3.67 μV and 0.0127 ± 0.0006 (CI), respectively. Figure 3I,J shows the statistics of the EFP interval and MB interval. From the results, it can be found that both these parameters increased with time, meaning the reduction of the firing rate. Moreover, to visualize the features of cardiac rhythm variability, a Poincaré plot was introduced to characterize the changes in the signal interval of cardiomyocytes.[28] As shown in Figure 3K, the data of recorded signals from different days distributed along a line with a slope of 1, and the distance between the data of different days and the origin of the coordinate is getting farther with time. Therefore, considering the cell physiological status and stability of signal recording, days 5−6 were usually determined as the appropriate time for bitter tests.

Bitter Compound Analysis by the Hybrid Integrated Cardiomyocyte Biosensor. RT-qPCR results above have demonstrated the expression of bitter receptors in cardiomyocytes, including seven bitter receptors (Tas2r108, Tas2r120, Tas2r121, Tas2r126, Tas2r135, Tas2r137, Tas2r143). According to a bitter database (Bitter DB),[29] four typical bitter compounds (Dena, diphenidol, quinine, arbutin) that can activate the bitter receptors in cardiomyocytes were chosen to verify the performance of HICB. Among these four bitter compounds, Dena can activate Tas2r135; diphenidol activates Tas2r108 and Tas2r137; quinine activates Tas2r108, Tas2r126, and Tas2r137; and arbutin activates Tas2r126 and Tas2r143.[30] All bitter compounds were configured to 100 μM solutions and preheated to 37 °C before being added to the HICB platform.

The quick response signals to bitter compounds of cardiomyocytes were recorded by HICB in real time. Figure 4A shows the typical electromechanical signals of cardiomyocytes treated with different bitter compounds after 5 min. It can be found that both the EFP and MB signals of cardiomyocytes changed significantly, and different bitter compounds presented different signal patterns. For example, the electromechanical signals of cardiomyocytes treated with Dena and quinine showed similar patterns, where the firing rate of cardiomyocytes decreased significantly, while the MB amplitude increased. The diphenidol treatment group presented a relatively mild effect on signal responses, decreasing in terms of both the firing rate and EFP amplitude and increasing slightly in terms of the MB amplitude. In contrast, the signals after treatment with arbutin presented irregular signal intervals, showing arrhythmic features.

To further investigate the differences of signal interval treated by different bitter compounds, Poincaré plots were presented to display the different effects of bitter compounds on cardiomyocytes. From the results (Figure 4B), it can be found that the control group and the data from cardiomyocytes treated with Dena, diphenidol, and quinine distributed along a line with a slope of 1, while the data from cardiomyocytes treated with arbutin was scattered, indicating that the signal interval of first three bitter compounds was regular, while arbutin presented an irregular signal interval. Furthermore, the distance between diphenidol distribution and the control group is shorter, demonstrating that the signal intervals of diphenidol change slightly compared with those of the control group. Meanwhile, there is some overlap in the distribution of Dena and quinine, indicating that these two bitter compounds show similar signal interval changes, which can be verified by typical electromechanical signals and statistics mentioned above. In contrast, the distance between the data from cardiomyocytes treated with arbutin and the control group is greater and distributed disorderly, indicating slow heart rate and arrhythmia.

Moreover, to quantify the differences among different signal responses, 15 different feature parameters of signals defined above were extracted, whose normalized statistics are shown in Figure 4C,D (control data were set as 1.0). From the statistics, it can be found that the firing rate, EFP amplitude, MB amplitude, EFP interval, and MB interval in Figure 4C changed more dramatically compared with other parameters in Figure 4D. To be specific, the firing rate and EFP amplitude decreased after treatment with all bitter compounds, while the MB amplitude, EFP interval, and MB interval all increased significantly after treatment with bitter compounds. In addition, the duration time between different feature points displayed various change patterns. For instance, E1−E2 of diphenidol and E3−M1 of quinine decreased significantly compared with those of the control group, while most of the other parameters presented varying degrees of increase.

Although the statistics of different parameters of cardiomyocytes after different bitter compounds treatment have been shown above, the representation of the histogram is not obvious enough to show subtle differences between bitter compounds. Thus, to display the data features more intuitively, the radar map and heat map were introduced to visualize the extracted parameters of cardiomyocytes after bitter treatment. As shown in the radar map (Figure 4E), all extracted parameters were integrated for comparison in the same map, where the control group was set as black enneagon labeled 1. All bitter treatment groups shrank in terms of the firing rate and EFP amplitude, while presented obvious spread in terms of MB amplitude, EFP interval, and MB interval. In the radar map, each bitter compound has its specific pattern compared with the control group, and the radar map can intuitively reflect visualization responses of cardiomyocytes to different bitter compounds.

Furthermore, the specific responses to different bitter compounds were distinct compared with the control group in the heat map, as shown in Figure 4F. The region labeled red means increase, while the blue region means decrease. It can be found that the firing rate and EFP amplitude of these four bitter compounds all presented blue, indicating a decrease in these two parameters. Rest parameters, MB amplitude, EFP interval, and MB interval of Dena regions, as well as EFP interval and MB interval of arbutin regions, showed dark red, indicating a large increase. In the regions of E3-M2 duration, quinine presented blue, while other bitter compounds displayed light red, implying the different changes of quinine.

Moreover, these extracted parameters were further used for bitter clustering. PCA was employed to discriminate the specific response of cardiomyocytes to different bitter compounds for visualized bitter clustering. Figure 4G shows the 2D pattern clustering results based on the first two principal components, whose weight coefficients are 58.78 and 18.4%, respectively. All data were clustered into five regions, and the data of the control group, Dena, diphenidol, and quinine distributed in the same region, while the data distribution of arbutin was the widest compared with other bitter compounds. The average Euclidean distances from Dena, diphenidol, quinine, and arbutin to the control group were 4.55, 3.51, 3.20, and 5.60, respectively. The results

https://doi.org/10.1021/acssensors.1c00158
ACS Sens. 2021, 6, 2593−2604

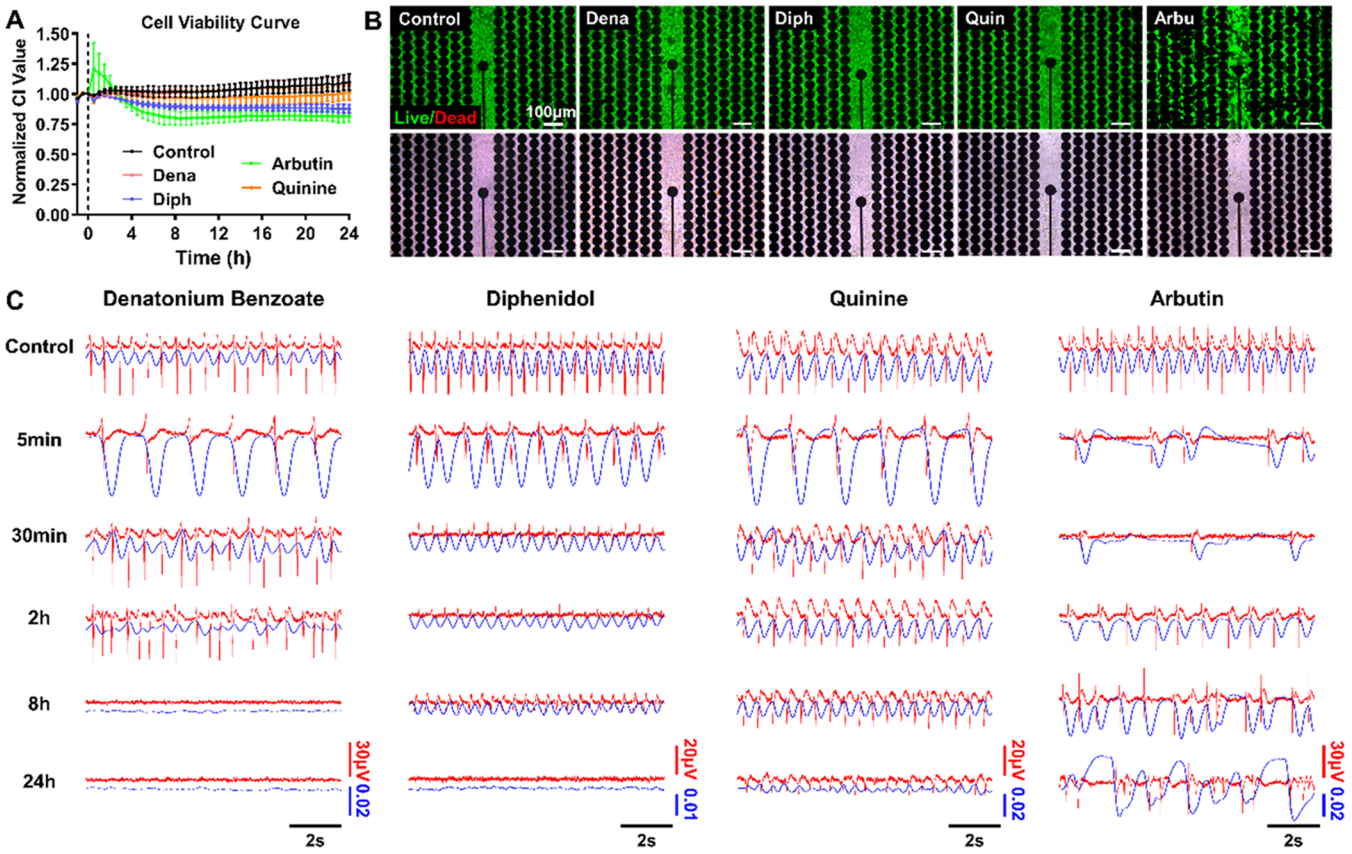

Figure 5. Cardiomyocytes' response to different bitter compounds. (A) Normalized cell viability curves after treatment with different bitter compounds, (B) live/dead staining results of cardiomyocytes after treatment with different bitter compounds for 24 h, and (C) typical electromechanical signals of cardiomyocytes treated with different bitter compounds at different recording times.

demonstrate that the signal responses of HICB to different bitter compounds can be effectively clustered by PCA.

Long-Term Cardiotoxicity Assessment of Bitter Compounds. From the results above, it was demonstrated that bitter compounds can activate the bitter receptors in cardiomyocytes, whose quick responses to different bitter compounds can be recorded by HICB. As we know, bitter compounds usually have toxicity. Therefore, the long-term cardiotoxicity induced by bitter compounds also was evaluated by HICB. Here, the cell viability and EFP and MB signals after bitter treatment were synchronously recorded within 24 h.

From the results of cell growth curves and live/dead staining (Figure 5A,B), all of these four bitter compounds have no significant side effect on the cell viability of cardiomyocytes during 24 h, thus excluding the possibility of affecting the electromechanical properties of cardiomyocytes through cell viability. The electrophysiological responses of cardiomyocytes to different bitter compounds were recorded by HICB in real time. Figure 5C shows the typical electromechanical signals of cardiomyocytes after applying different bitter compounds during the recording period. It can be found that both EFP and MB signals of cardiomyocytes changed significantly with time and different bitter compounds displayed different signal patterns. For example, the electromechanical signals of cardiomyocytes treated with Dena and diphenidol were gradually inhibited as time goes by and even totally disappeared at 8 and 24 h, respectively. Quinine presented a relatively mild effect on signal responses, while the signals after treatment with arbutin showed some arrhythmic features.

To further investigate the differences among different signal responses, different feature parameters of signals including the firing rate, EFP amplitude, MB amplitude, EFP interval, MB interval, E1−E2 duration, E1−E3 duration, E2−M1 duration, and M1−M2 duration were extracted, whose normalized statistics are shown in Figure 6A (control data were set as 1.0). From the statistics, it can be found that the firing rate, EFP amplitude, MB amplitude, EFP interval, and MB interval changed more dramatically compared with other parameters, which also can be observed from the heat maps in Figure 6B. In addition, Poincaré plots were presented to clarify the effects of different bitter compounds on the signal interval of cardiomyocytes (Figure 6C). From the results, it can be found that the data after treatment with Dena and quinine distributed along a line with a slope of 1, and the data after treatment with diphenidol distributed more widely, while the signal distribution of arbutin was completely disorganized. Moreover, power spectral density (PSD) diagrams were introduced to display the energy changes at different moments after treatment with bitter compounds. From Figure 6D, it can be found that almost all of the power of EFP signals decreased after treatment with bitter compounds. To be specific, the power of EFP signals after treatment with Dena and quinine decreased first, then increased again, and finally decreased at 24 h (Figure 6E). The power of the EFP signal after treatment with diphenidol was declining almost all of the time, while that of arbutin reached its minimum at 2 h and then started to recover. Similarly, the PSD diagrams and statistics of MB signals are shown in Figure 6F,6G. From the PSD diagrams of

https://doi.org/10.1021/acssensors.1c00158
ACS Sens. 2021, 6, 2593−2604

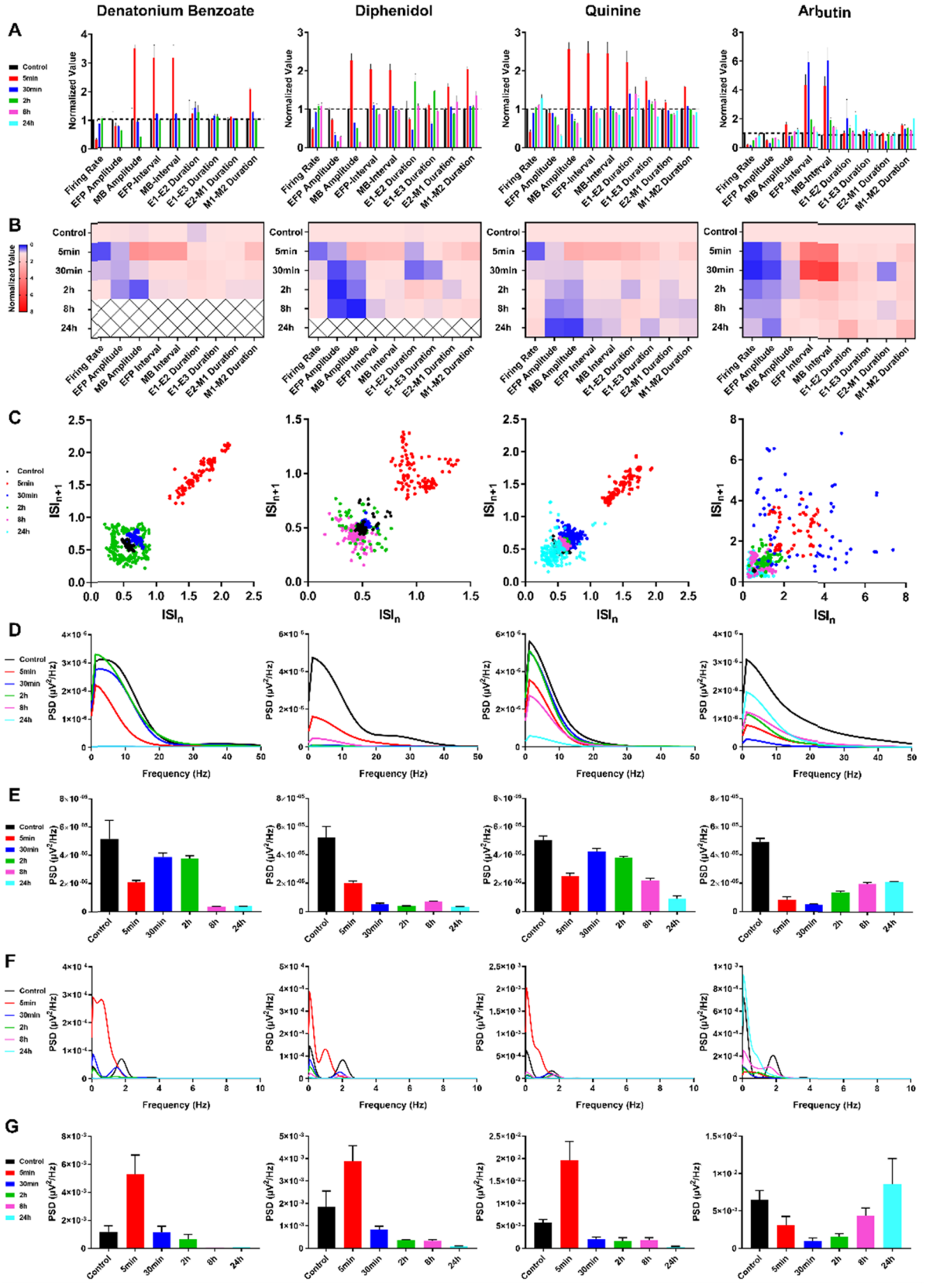

Figure 6. Signal analysis of the hybrid integrated cardiomyocyte biosensor (HICB) to different bitter compounds at different recording times. (A) Normalized statistics of extracted parameters; (B) visualized heat maps of extracted parameters, n = 3; (C) Poincaré plots of data treated by different bitter compounds; (D) power spectral density (PSD) diagrams of EFP signals from HICB treated by different bitter compounds at different recording times; (E) PSD statistics of EFP signals after treatment with different bitter compounds, n = 3; (F) PSD diagrams of MB signals after treatment with different bitter compounds at different recording times; and (G) PSD statistics of MB signals after treatment with different bitter compounds, n = 3.

https://doi.org/10.1021/acssensors.1c00158
ACS Sens. 2021, 6, 2593−2604

MB signals, it can be found that the power of MB signals increased after 5 min treatment with Dena, diphenidol, and quinine, and then decreased with time. The power of the MB signal after treatment with arbutin showed a decrease for the first 30 min and then kept increasing.

In terms of long-term toxicity, Dena, diphenidol, and quinine all showed inhibition effects on electrophysiological activity and mechanical beating of cardiomyocytes, while the cardiomyocytes treated with arbutin displayed some arrhythmic characteristics. Therefore, the HICB established in this study can be used to evaluate the long-term cardiotoxicity and side effects of bitter compounds.

DISCUSSION

In this study, a HICB was established to synchronously record the EFP and MB signals of cardiomyocytes, which has advantages in noninvasive, long-term, and high-throughput recording. This HICB platform was used to investigate the effects of bitter compounds on the electromechanical signal of cardiomyocytes for bitter detection and cardiotoxicity assessment.

GPCRs are seven transmembrane-spanning proteins and can mediate the taste sensations of bitter, sweet, and umami among five taste sensations.[13] Among these different GPCRs, the taste receptor type 1 (T1rs) family mediates sweet and umami taste, while taste receptor type 2 (T2rs) mediates bitter taste.[2] In recent years, researchers have demonstrated that taste receptors are expressed in not only the gustatory system but also other nongustatory tissues and organs such as the brain and gastrointestinal and respiratory tracts of mammals.[17,31−33] Remarkably, Foster et al. reported that T1rs and T2rs were expressed in neonatal whole rat hearts for the first time.[34] For the bitter receptors specifically, the expression levels of T2r108, T2r120, T2r121, T2r126, T2r135, T2r137, and T2r143 were notably higher than other bitter receptors. Our RT-qPCR results also confirmed that seven bitter receptors (T2r108, T2r120, T2r121, T2r126, T2r135, T2r137, and T2r143) were expressed in the rat cardiomyocytes.

Cardiomyocytes possess unique electromechanical behavior based on the ECC process, where Ca^{2+} serves as a bridge to link electrical excitation and mechanical contraction of cardiomyocytes and convert the chemical signals to the final mechanical contraction of cardiomyocytes. During the ECC process, the excitation of cardiomyocytes leads to the opening of voltage-dependent L-type Ca^{2+} channels on the cell membrane and induces the influx of extracellular Ca^{2+}, leading to a large amount of Ca^{2+} released from the sarcoplasmic reticulum into the cytoplasm. This immediate increase of Ca^{2+} concentration in the cytoplasm is called as Ca^{2+} transient.[35] Based on our Ca^{2+} imaging and optical recording results, bitter compounds showed an inhibition effect on the frequency of calcium activities, meaning that the ECC of cardiomyocytes can be inhibited by bitter compounds, and this result was consistent with former studies.[21,22] Therefore, bitter compounds might regulate the function of the heart by activating the bitter receptors in cardiomyocytes.

With the special and interesting effects of bitter compounds on cardiomyocytes, it is particularly important and necessary to define its signaling transduction pathway. Nevertheless, the precise signaling transduction pathway of bitter receptors T2Rs in the heart remains unclear.[36] According to the current classical bitter taste signaling transduction pathway, the binding of bitter ligands to T2Rs leads to a conformation change in the receptor, allowing it to interact with $G_{\alpha\text{-Gustducin}}$ and $G_{\beta\gamma}$,[37] which can activate subsequent downstream pathways.[38] Through activating the phosphodiesterases (PDE), $G_{\alpha\text{-Gustducin}}$ can decrease the levels of cAMP, which can lead to the increase of intracellular Ca^{2+}. In another pathway, $G_{\beta\gamma}$ can activate PLCβ2, producing two intracellular messengers, IP_3 and diacylglycerol (DAG). IP_3 can activate IP_3R3 of the endoplasmic reticulum to release Ca^{2+}, causing an increase in intracellular Ca^{2+}. Thus, both pathways lead to an increase of intracellular Ca^{2+}, which then activates the Ca^{2+}-dependent TRPM5 channels. Subsequently, the plasma membrane depolarizes to produce action potentials and release ATP.[13,39] However, there is limited evidence for the presence of all classical taste signaling components in the heart.[36] For example, Gγ13 and TRPM5 have not been observed in human heart tissues from previous studies,[37,40] which are considered necessary for taste signal transduction. Hence, bitter agonists might mediate the T2Rs in cardiomyocytes in other pathways. Foster et al. demonstrated that T2Rs agonist-induced changes in heart function are G-protein-dependent by exerting $G_{\alpha i}$ and $G_{\beta\gamma}$ inhibitors (pertussis toxin and gallein).[21] Xin et al. provided possible mechanism evidence that T2Rs agonists can activate PDE through $G_{\alpha\text{-Gustducin}}$, leading to a decrease of cAMP, and thus inhibit the cardiac contractions by attenuating the L-type Ca^{2+} channels and the consequent Ca^{2+} release.[22,41]

Though there is no clear consensus on the precise mechanism of signaling transduction pathways of T2Rs in cardiomyocytes, it is an agreement that bitter agonists can mediate contractile responses in the cardiovascular system.[36] For instance, Foster et al. identified novel agonist ligands for cardiac-T2Rs and observed dose-dependent negative inotropic effects in response to bitter ligands in the experiments of Langendorff-perfused mouse hearts.[21,22] Yuan et al. reported that T2Rs agonists, quinine and chloroquine, could decrease the heart rate and increased the RR interval and QRS duration in Langendorff-perfused isolated rat hearts.[22] In our work, inhibition effects of bitter agonists on both the electrophysiological and contractile activity of cardiomyocytes can be observed, which might be attributed to the changes in ion channels (Na^+, K^+, Ca^{2+}) on cell membranes caused by intermediate signaling components produced after activation of bitter taste receptors.[5,42]

In addition, the role of bitter taste is commonly assumed to signal toxicity as we know, which can alert animals against consuming harmful compounds.[5] About 60% of the bitter compounds have documented toxicity.[23] Therefore, in addition to the activation process of bitter receptors T2Rs, the long-term cumulative toxicity on the heart induced by bitter agonists cannot be ignored. Here, cardiotoxicity induced by bitter agonists was also chronically evaluated by HICB in this work. According to the long-term recording results, these bitter compounds presented an inhibition effect on the electrophysiological and contractile activities of cardiomyocytes.

Dena is regarded as the most bitter compound in nature and can cause a strong bitter response in even very small doses. We found that the electrophysiological and contractile activity of cardiomyocytes almost completely stopped within 8h without affecting the cell viability. It is noteworthy that when Dena was eluted, the electrophysiological and contractile activity of cardiomyocytes recovered to almost normal levels, suggesting that the presence of the Dena temporarily inhibited the activity of associated ion channels. Diphenidol is usually used as an antiemetic and antivertigo drug, whose mechanism remains not

https://doi.org/10.1021/acssensors.1c00158
ACS Sens. 2021, 6, 2593−2604

entirely clear. Leung et al. reported that diphenidol can block the neuronal voltage-gated ion channels (Na^+, K^+, and Ca^{2+}) in neuronal cells.[43] Besides, previous researchers have reported that 1×10^{-5} M diphenidol resulted in depression of total action potential amplitude (−11%), and toxic concentrations of diphenidol (1×10^{-4} M) resulted in further depression,[44] whose inhibition effect is consistent with our research results. Quinine is important for severe malaria treatment as an antimalarial drug.[45] However, cardiotoxicity is the common adverse effect during quinine treatment.[46] Previous studies have reported the electrophysiological effect of quinine on the heart. For example, Kinoshita et al. found that quinine prolonged the electrocardiographic QT interval in a dose-dependent manner in the isolated perfused guinea pig heart.[47] Touze et al. reported that quinine induced a significant decrease in the QT/RR slope in the patients with malaria by measuring the surface electrocardiograms.[48] Consistent with reported results of QT interval prolongation, we also observed the reduction of electrophysiological activity after quinine treatment, which may be associated with the time-dependent blockage of the hERG (human ether-a-go-go-related gene) potassium channel of quinine.[49] Interestingly, arbutin showed the side effect of arrhythmia, whose mechanism is yet unclear and needs further study.

CONCLUSIONS

In this work, we established a HICB for bitter compound detection and cardiotoxicity assessment. The expression of T2Rs in cardiomyocytes was confirmed by RT-qPCR. By performing Ca^{2+} imaging and optical video recording, it is demonstrated that bitter compounds can affect the Ca^{2+} influx and beating status of cardiomyocytes. Neonatal rat cardiomyocytes were selected as a sensitive element to build a HICB for bitter detection and cardiotoxicity assessment, where the electromechanical signals of cardiomyocytes can be recorded synchronously. Four bitter compounds (Dena, diphenidol, quinine, and arbutin) that can activate different bitter receptors in cardiomyocytes were administrated and the quick responses of HICB were recorded for bitter detection. To explore the more details of recorded electromechanical signals, feature points were defined and 15 feature parameters were extracted, which were visualized by a radar map and heat map. The data treated by different bitter compounds can be further clustered by PCA. Moreover, the long-term cardiotoxicity of bitter compounds was also evaluated by HICB. Four types of bitter compounds presented varying degrees of inhibition effect on the electrophysiological and contractile activity of cardiomyocytes. In summary, this study provides a new strategy for bitter detection and long-term cardiotoxicity assessment, showing promising applications in taste detection and toxicity screening.

ASSOCIATED CONTENT

Supporting Information

The Supporting Information is available free of charge at https://pubs.acs.org/doi/10.1021/acssensors.1c00158.

Fabrication process and pictures of the hybrid integrated biosensor and gene-specific primers used in the RT-qPCR experiment (PDF)

AUTHOR INFORMATION

Corresponding Authors

Liujing Zhuang − *Biosensor National Special Laboratory, Key Laboratory for Biomedical Engineering of Education Ministry, Department of Biomedical Engineering, Zhejiang University, Hangzhou 310027, China*; Email: thisiszlj@163.com

Ning Hu − *State Key Laboratory of Optoelectronic Materials and Technologies, Guangdong Province Key Laboratory of Display Material and Technology, School of Electronics and Information Technology, Sun Yat-sen University, Guangzhou 510006, China*; orcid.org/0000-0001-7178-3952; Email: huning3@mail.sysu.edu.cn

Ping Wang − *Biosensor National Special Laboratory, Key Laboratory for Biomedical Engineering of Education Ministry, Department of Biomedical Engineering, Zhejiang University, Hangzhou 310027, China*; orcid.org/0000-0001-6474-2722; Phone: 0571-87952832; Email: cnpwang@zju.edu.cn

Authors

Xinwei Wei − *Biosensor National Special Laboratory, Key Laboratory for Biomedical Engineering of Education Ministry, Department of Biomedical Engineering, Zhejiang University, Hangzhou 310027, China*

Deming Jiang − *Biosensor National Special Laboratory, Key Laboratory for Biomedical Engineering of Education Ministry, Department of Biomedical Engineering, Zhejiang University, Hangzhou 310027, China*

Changming Chen − *Biosensor National Special Laboratory, Key Laboratory for Biomedical Engineering of Education Ministry, Department of Biomedical Engineering, Zhejiang University, Hangzhou 310027, China*

Jianguo Wu − *Biosensor National Special Laboratory, Key Laboratory for Biomedical Engineering of Education Ministry, Department of Biomedical Engineering, Zhejiang University, Hangzhou 310027, China*

Chunlian Qin − *Biosensor National Special Laboratory, Key Laboratory for Biomedical Engineering of Education Ministry, Department of Biomedical Engineering, Zhejiang University, Hangzhou 310027, China*

Qunchen Yuan − *Biosensor National Special Laboratory, Key Laboratory for Biomedical Engineering of Education Ministry, Department of Biomedical Engineering, Zhejiang University, Hangzhou 310027, China*

Yingying Xue − *Biosensor National Special Laboratory, Key Laboratory for Biomedical Engineering of Education Ministry, Department of Biomedical Engineering, Zhejiang University, Hangzhou 310027, China*

Yizhou Xiong − *Biosensor National Special Laboratory, Key Laboratory for Biomedical Engineering of Education Ministry, Department of Biomedical Engineering, Zhejiang University, Hangzhou 310027, China*

Complete contact information is available at: https://pubs.acs.org/10.1021/acssensors.1c00158

Notes

The authors declare no competing financial interest.

ACKNOWLEDGMENTS

This work was supported by the National Natural Science Foundation of China (31627801, 51861145307, 61901412,

and 31800826), Major Research and Development Project of Zhejiang Province (2019C03066), the Department of Science and Technology of Guangdong Province Project (2020B1212060030), Guangdong Basic and Applied Basic Research Foundation (2020A1515010665), and the National Postdoctoral Program for Innovative Talent of China (BX2021265). The authors thank Dr. Jingwen Liu for her kind help in RT-qPCR experiments and also thank Jian Wu and Xin Yao from ACEA Biosciences for their help in the fabrication of the sensor and detection system.

REFERENCES

(1) Chaudhari, N.; Roper, S. D. Review series: The cell biology of taste. *J. cell biol.* **2010**, *190*, 285−296.
(2) Chandrashekar, J.; Hoon, M. A.; Ryba, N. J.; Zuker, C. S. The receptors and cells for mammalian taste. *Nature* **2006**, *444*, 288−294.
(3) Chaudhari, N.; Roper, S. D. The cell biology of taste. *J. cell biol.* **2010**, *190*, 285−296.
(4) Behrens, M.; Meyerhof, W. Vertebrate bitter taste receptors: keys for survival in changing environments. *J. Agric. Food Chem.* **2018**, *66*, 2204−2213.
(5) Avau, B.; Depoortere, I. The bitter truth about bitter taste receptors: beyond sensing bitter in the oral cavity. *Acta Physiol.* **2016**, *216*, 407−420.
(6) Tahara, Y.; Toko, K. Electronic tongues−a review. *IEEE Sens. J.* **2013**, *13*, 3001−3011.
(7) Vlasov, Y.; Legin, A.; Rudnitskaya, A. Electronic tongues and their analytical application. *Anal. Bioanal. Chem.* **2002**, *373*, 136−146.
(8) Riul, A., Jr.; Dantas, C. A.; Miyazaki, C. M.; Oliveira, O. N., Jr. Recent advances in electronic tongues. *Analyst* **2010**, *135*, 2481−2495.
(9) Escuder-Gilabert, L.; Peris, M. Highlights in recent applications of electronic tongues in food analysis. *Anal. Chim. Acta* **2010**, *665*, 15−25.
(10) Wasilewski, T.; Kamysz, W.; Gębicki, J. Bioelectronic tongue: Current status and perspectives. *Biosens. Bioelectron.* **2020**, *150*, No. 111923.
(11) Cetó, X.; Voelcker, N. H.; Prieto-Simón, B. Bioelectronic tongues: New trends and applications in water and food analysis. *Biosens. Bioelectron.* **2016**, *79*, 608−626.
(12) Roper, S. D. Taste buds as peripheral chemosensory processors. *Semin. Cell Dev. Biol.* **2013**, 71−79.
(13) Zhang, Y.; Hoon, M. A.; Chandrashekar, J.; Mueller, K. L.; Cook, B.; Wu, D.; Zuker, C. S.; Ryba, N. J. Coding of sweet, bitter, and umami tastes: different receptor cells sharing similar signaling pathways. *Cell* **2003**, *112*, 293−301.
(14) Hu, L.; Xu, J.; Qin, Z.; Hu, N.; Zhou, M.; Huang, L.; Wang, P. Detection of bitterness in vitro by a novel male mouse germ cell-based biosensor. *Sens. Actuators, B* **2016**, *223*, 461−469.
(15) Tian, Y.; Zhu, P.; Chen, Y.; Chen, W.; Du, L.; Wu, C.; Wang, P. A sperm-cell-based biosensor using a fluorescence probe for responsive signal readout toward bitter flavor detection. *Talanta* **2020**, *211*, No. 120731.
(16) Qin, C.; Qin, Z.; Zhao, D.; Pan, Y.; Zhuang, L.; Wan, H.; Di Pizio, A.; Malach, E.; Niv, M. Y.; Huang, L.; Hu, N.; Wang, P. A bioinspired in vitro bioelectronic tongue with human T2R38 receptor for high-specificity detection of NC = S-containing compounds. *Talanta* **2019**, *199*, 131−139.
(17) Xu, J.; Cao, J.; Iguchi, N.; Riethmacher, D.; Huang, L. Functional characterization of bitter-taste receptors expressed in mammalian testis. *MHR: Basic Sci. Reprod. Med.* **2012**, *19*, 17−28.
(18) Wu, S. V.; Rozengurt, N.; Yang, M.; Young, S. H.; Sinnett-Smith, J.; Rozengurt, E. Expression of bitter taste receptors of the T2R family in the gastrointestinal tract and enteroendocrine STC-1 cells. *Proc. Natl. Acad. Sci. U.S.A.* **2002**, *99*, 2392−2397.
(19) Hu, L.; Zou, L.; Qin, Z.; Fang, J.; Huang, L.; Wang, P. A novel label-free bioengineered cell-based biosensor for salicin detection. *Sens. Actuators, B* **2017**, *238*, 1151−1158.
(20) Wei, X.; Qin, C.; Gu, C.; He, C.; Yuan, Q.; Liu, M.; Zhuang, L.; Wan, H.; Wang, P. A novel bionic in vitro bioelectronic tongue based on cardiomyocytes and microelectrode array for bitter and umami detection. *Biosens. Bioelectron.* **2019**, *145*, No. 111673.
(21) Foster, S. R.; Blank, K.; Hoe, L. E. S.; Behrens, M.; Meyerhof, W.; Peart, J. N.; Thomas, W. G. Bitter taste receptor agonists elicit G-protein-dependent negative inotropy in the murine heart. *FASEB J.* **2014**, *28*, 4497−4508.
(22) Yuan, G.; Jing, Y.; Wang, T.; Fernandes, V. S.; Xin, W. The bitter taste receptor agonist-induced negative chronotropic effects on the Langendorff-perfused isolated rat hearts. *Eur. J. Pharmacol.* **2020**, *876*, No. 173063.
(23) Nissim, I.; Dagan-Wiener, A.; Niv, M. Y. The taste of toxicity: A quantitative analysis of bitter and toxic molecules. *IUBMB Life* **2017**, *69*, 938−946.
(24) Li, H.; Fang, J.; Xinwei, W.; Xu, D.; Zhang, T.; Xiang, Y.; Chen, H.-J.; Liu, F.; Xie, X.; Wang, P. Specific recognition of ion channel blocker by high-content cardiomyocyte electromechanical integrated correlation. *Biosens. Bioelectron.* **2020**, No. 112273.
(25) Wei, X.; Zhuang, L.; Li, H.; He, C.; Wan, H.; Hu, N.; Wang, P. Advances in Multidimensional Cardiac Biosensing Technologies: From Electrophysiology to Mechanical Motion and Contractile Force. *Small* **2020**, *16*, No. 2005828.
(26) Wei, X.; Gao, Q.; Xie, C.; Gu, C.; Liang, T.; Wan, H.; Zhuang, L.; He, Y.; Wang, P. Extracellular recordings of bionic engineered cardiac tissue based on a porous scaffold and microelectrode arrays. *Anal. Methods* **2019**, *11*, 5872−5879.
(27) Wei, X.; Gu, C.; Li, H.; Pan, Y.; Zhang, B.; Zhuang, L.; Wan, H.; Hu, N.; Wang, P. Efficacy and cardiotoxicity integrated assessment of anticancer drugs by a dual functional cell-based biosensor. *Sens. Actuators, B* **2019**, *283*, 881−889.
(28) Khandoker, A. H.; Karmakar, C.; Brennan, M.; Palaniswami, M.; Voss, A. *Poincaré plot methods for heart rate variability analysis.* Springer, 2013.
(29) Wiener, A.; Shudler, M.; Levit, A.; Niv, M. Y. BitterDB: a database of bitter compounds. *Nucleic Acids Res.* **2012**, *40*, D413−D419.
(30) Lossow, K.; Hübner, S.; Roudnitzky, N.; Slack, J. P.; Pollastro, F.; Behrens, M.; Meyerhof, W. Comprehensive analysis of mouse bitter taste receptors reveals different molecular receptive ranges for orthologous receptors in mice and humans. *J. Biol. Chem.* **2016**, *291*, 15358−15377.
(31) Bezençon, C.; Le Coutre, J.; Damak, S. Taste-signaling proteins are coexpressed in solitary intestinal epithelial cells. *Chem. senses* **2007**, *32*, 41−49.
(32) Tizzano, M.; Cristofoletti, M.; Sbarbati, A.; Finger, T. E. Expression of taste receptors in solitary chemosensory cells of rodent airways. *BMC Pulm. Med.* **2011**, *11*, No. 3.
(33) Singh, N.; Vrontakis, M.; Parkinson, F.; Chelikani, P. Functional bitter taste receptors are expressed in brain cells. *Biochem. Biophys. Res. Commun.* **2011**, *406*, 146−151.
(34) Foster, S. R.; Porrello, E. R.; Purdue, B.; Chan, H.-W.; Voigt, A.; Frenzel, S.; Hannan, R. D.; Moritz, K. M.; Simmons, D. G.; Molenaar, P.; et al. Expression, regulation and putative nutrient-sensing function of taste GPCRs in the heart. *PLoS One* **2013**, *8*, No. e64579.
(35) Bers, D. M. Cardiac excitation−contraction coupling. *Nature* **2002**, *415*, 198−205.
(36) Bloxham, C. J.; Foster, S. R.; Thomas, W. G. A Bitter Taste in Your Heart. *Front. Plant Physiol.* **2020**, *11*, No. 431.
(37) Huang, L.; Shanker, Y. G.; Dubauskaite, J.; Zheng, J. Z.; Yan, W.; Rosenzweig, S.; Spielman, A. I.; Max, M.; Margolskee, R. F. Gγ13 colocalizes with gustducin in taste receptor cells and mediates IP 3 responses to bitter denatonium. *Nat. Neurosci.* **1999**, *2*, 1055−1062.
(38) Yan, W.; Sunavala, G.; Rosenzweig, S.; Dasso, M.; Brand, J. G.; Spielman, A. I. Bitter taste transduced by PLC-β2-dependent rise in IP3 and α-gustducin-dependent fall in cyclic nucleotides. *Am. J. Physiol.: Cell Physiol.* **2001**, *280*, C742−C751.

https://doi.org/10.1021/acssensors.1c00158
ACS Sens. 2021, 6, 2593−2604

(39) Taruno, A.; Vingtdeux, V.; Ohmoto, M.; Ma, Z.; Dvoryanchikov, G.; Li, A.; Adrien, L.; Zhao, H.; Leung, S.; Abernethy, M.; et al. CALHM1 ion channel mediates purinergic neurotransmission of sweet, bitter and umami tastes. *Nature* **2013**, *495*, 223−226.
(40) Demir, T.; Yumrutas, O.; Cengiz, B.; Demiryurek, S.; Unverdi, H.; Kaplan, D. S.; Bayraktar, R.; Ozkul, N.; Bagcı, C. Evaluation of TRPM (transient receptor potential melastatin) genes expressions in myocardial ischemia and reperfusion. *Mol. Biol. Rep.* **2014**, *41*, 2845−2849.
(41) Xin, W.; Wang, T.; Jing, Y.; Fernandes, V. S. L. The novel mechanism of bitter taste receptors attenuating rat ventricular contractility. *FASEB J.* **2018**, *32*, No. 839.10.
(42) Huang, H.; Pugsley, M. K.; Fermini, B.; Curtis, M. J.; Koerner, J.; Accardi, M.; Authier, S. Cardiac voltage-gated ion channels in safety pharmacology: review of the landscape leading to the CiPA initiative. *J. Pharmacol. Toxicol. Methods* **2017**, *87*, 11−23.
(43) Leung, Y.-M.; Wong, K.-L.; Cheng, K.-S.; Kuo, C.-S.; Su, T.-H.; Chen, Y.-W.; Cheng, T.-H. Inhibition of voltage-gated K+ channels and Ca 2+ channels by diphenidol. *Pharmacol. Rep.* **2012**, *64*, 739−744.
(44) Hayakawa, H.; Mandel, W. J. Electrophysiologic effects of diphenidol in isolated cardiac tissue. *J. Pharmacol. Exp. Ther.* **1973**, *185*, 447−456.
(45) Achan, J.; Talisuna, A. O.; Erhart, A.; Yeka, A.; Tibenderana, J. K.; Baliraine, F. N.; Rosenthal, P. J.; D'Alessandro, U. Quinine, an old anti-malarial drug in a modern world: role in the treatment of malaria. *Malar. J.* **2011**, *10*, No. 144.
(46) Bonington, A.; Davidson, R. N.; Winstanley, P. A.; Pasvol, G. Fatal quinine cardiotoxicity in the treatment of falciparum malaria. *Trans. R. Soc. Trop. Med. Hyg.* **1996**, *90*, 305−307.
(47) Kinoshita, A.; Yamada, H.; Kotaki, H.; Kimura, M. Effects of anti-malarial drugs on the electrocardiographic QT interval modelled in the isolated perfused guinea pig heart system. *Malar. J.* **2010**, *9*, No. 318.
(48) Touze, J.; Heno, P.; Fourcade, L.; Deharo, J.; Thomas, G.; Bohan, S.; Paule, P.; Riviere, P.; Kouassi, E.; Buguet, A. The effects of antimalarial drugs on ventricular repolarization. *Am. J. Trop. Med. Hyg.* **2002**, *67*, 54−60.
(49) Yan, M.; Fan, P.; Shi, Y.; Feng, L.; Wang, J.; Zhan, G.; Li, B. Stereoselective blockage of quinidine and quinine in the hERG channel and the effect of their rescue potency on drug-induced hERG trafficking defect. *Int. J. Mol. Sci* **2016**, *17*, No. 1648.

https://doi.org/10.1021/acssensors.1c00158
ACS Sens. 2021, 6, 2593−2604